

Article

# Novel Material Obtained from the Gasification Residues of Candiota Mine's Coal for Cationic Dye Adsorption

Gabriella Lucena<sup>1</sup>, Tereza Longaray Rodrigues<sup>2</sup>, Josué Vieira da Rosa<sup>1</sup>, Gabriela Silveira da Rosa<sup>1,2</sup>   
and Ana Rosa Costa Muniz<sup>1,\*</sup>

<sup>1</sup> Chemical Engineering, Federal University of Pampa, Bagé 96413-172, RS, Brazil

<sup>2</sup> Graduate Program in Science and Engineering of Materials, Federal University of Pampa, Bagé 96413-172, RS, Brazil

\* Correspondence: anamuniz@unipampa.edu.br; Tel.: +55-53-991768793

**Abstract:** This work aims to prepare and characterize the unburned carbon obtained from gasification residues and evaluate its application as an adsorbent for the removal of textile dye contaminants. The results of physical and chemical properties showed a specific mass of 2.05 g/cm<sup>3</sup>, surface area of 23.983 g/cm<sup>2</sup>, and diameter and pore volume of 0.844 nm and 2.262 cm<sup>3</sup>/g, respectively. These properties, along with the point of zero charge and chemical bonds present on the surface, favored the adsorption of cationic dyes. The adsorption results showed great potential for the removal of methylene blue, crystal violet, and basic fuchsin if compared with bromocresol green, and indigo carmine. The maximum removal values obtained for methylene blue were up to 99% and the kinetic adsorption was faster at the beginning of the process, reaching the equilibrium in less than 5 min. The results obtained through the adsorption isotherms showed a maximum adsorption capacity of 333.33 and 476.19 mg/g, at the temperature of 291 and 328 K, respectively. The satisfactory results showed that the use of unburned carbon is a cost-effective and eco-friendly alternative to reusing the residue from gasification and also contributes to the decontamination of watercourses.

**Keywords:** unburned carbon; textile dyes; fly ash; methylene blue; coal



**Citation:** Lucena, G.; Rodrigues, T.L.; da Rosa, J.V.; da Rosa, G.S.; Muniz, A.R.C. Novel Material Obtained from the Gasification Residues of Candiota Mine's Coal for Cationic Dye Adsorption. *Mining* **2023**, *3*, 271–283. <https://doi.org/10.3390/mining3020017>

Academic Editor: Yassine Taha

Received: 9 March 2023

Revised: 18 April 2023

Accepted: 27 April 2023

Published: 5 May 2023



**Copyright:** © 2023 by the authors. Licensee MDPI, Basel, Switzerland. This article is an open access article distributed under the terms and conditions of the Creative Commons Attribution (CC BY) license (<https://creativecommons.org/licenses/by/4.0/>).

## 1. Introduction

Raw coal (RC) is a fossil fuel widely found in worldwide [1]. Brazil has an estimated coal reserve of 6.5996 billion tons and the largest mine is located in the south of Rio Grande do Sul, the Candiota mine [2,3]. The coal from this region is considered sub-bituminous, and is known for its high ash content, above 50% dry basis [4,5]. Although the main energy source in various countries is related to combustion, the use of coal has been decreasing to avoid the impact caused by greenhouse gas emissions [1], which is related to global warming. The climate change catastrophe requires the greatest attention and the use of clean technology in coal processing has been attracting significant investments.

Regarding the techniques that produce lower gas emissions, it is worth mentioning coal gasification [6]. Gasification is a thermochemical process that converts solid combustibles into liquid and gas products. The main product of coal gasification is syngas, which can be used to obtain other chemical products [1,7,8]. Some residues are produced by this process, such as ash, which can be classified as fly ash (FA) and bottom ash (BA). The FA are composed of small particles, presenting an average particle size between 3 to 34.57 µm, and are mainly composed of SiO<sub>2</sub>, Al<sub>2</sub>O<sub>3</sub>, Fe<sub>2</sub>O<sub>3</sub>, TiO<sub>2</sub>, CaO, and MgO [8–13]. The disposal of FA may be related to economic and environmental problems around the world, and thus researchers have been developing studies regarding its reuse, such as the synthesis of zeolite [12,14,15], development of a catalyst used in the decomposition of NO and NH<sub>3</sub> [16], recovery of gallium and vanadium [17], Zn<sup>2+</sup>, Pb<sup>2+</sup>, As (V), hexavalent chromium and dye

adsorption [11,18], and additive for the manufacture of cement, concrete, and concrete-admixed products. However, according to some authors, these applications may be limited since the proportion of unburned carbon (UC) can represent a barrier to its reuse [19–21].

UC is a material obtained through the incomplete gasification of coal, which is dragged with fly ash during the thermochemical process [1,22,23]. The morphology of this material differs from raw coal, as UC presents high porosity due to the heterogeneous reactions that cause changes in the particles' porous structure [8,24]. Thus, recent studies have been investigating some technologies used in the removal of UC from FA, which are classified as dry and wet separation methods. The wet methods basically consist of sieving, magnetic, gravitational, and electrostatic methods or a combination of them, while the dry methods are usually flotation and agglomeration [25–30]. The UC content may be related to some factors such as the nature of coal (particle size, mineral matter, calorific value, volatile matter, and others), the gasification conditions, and FA size [20,27].

In the last twenty years, researchers have been studying the application of UC in the treatment of aqueous and gaseous solutions, such as the adsorption of mercury [31], SO<sub>2</sub> [16], mordant orange [32], nitric oxide [33], methylene blue [24,32,34], Rhodamine B [24,32], crystal violet [24,34], acid black 1 [24], humic acid [35], and others. Adsorption has been extensively used for the removal of contaminants from water at different scales [36] which is widely used in the removal of contaminants from textile effluents [37,38]. The novelty of this study is the proposal of a new adsorbent material from an industrial residue and the evaluation of its application as an adsorbent for the removal of contaminants. Therefore, considering the potential applications of UC, the present study aims to recover the UC from FA, evaluate its physical and chemical properties, and its application in textile dye adsorption.

## 2. Materials and Methods

### 2.1. Production of Unburned Carbon (UC)

The UC was obtained from the fly ash produced by the gasification of coal from the Candiota-RS mine. The gasification process was carried out in a bench plant, with a capacity to process 10 kg of coal per hour, located in the Energy and Carbochemistry Laboratory (ECL) at the Federal University of Pampa, located 40 km from the Candiota mine. The process of separation of the UC contained in FA was executed in two steps. First, the samples were sieved (Bertel electromagnetic stirrer, Model VP-01, São Paulo, Brazil) to obtain a particle size between 2 and 0.053 mm. Subsequently, the particles of 0.250 mm were submitted to decantation using 250 mL of water and 10 g of sample. The top layer obtained was composed of fly ash, and the bottom layer was called unburned coal (UC). UC was dried at 105 °C for 24 h before the characterization and adsorption studies.

### 2.2. Characterization of UC

The characterization analyses of the UC are shown in Table 1.

**Table 1.** Physicochemical analysis of the UC.

Analysis	Type	Norm
Granulometric analysis	Physical	NBR 10850 [39]
Colorimetric analysis	Physical	NBR 10850 [39]
Calorimetric analysis	Physical	ASTM 1038.5 [40]
Gas pycnometry	Physical	NBR 12076 [41]
BET	Physical	-
FTIR	Chemical	ASTM E1252 [42]
XRF	Chemical	-

The colorimetric analysis was performed according to the CIELAB system using a colorimeter (Konica Minolta, model CM-2500d, Tokyo, Japan), and the sample was analyzed through the hue, brightness, and saturation. The calorimetric analysis was carried

out with a Parr 6200 oxygen bomb calorimeter. The determination of specific mass was obtained through gas pycnometry (Quantachrome Instruments, model Ultrapyc 1200e V4.01, Boynton Beach, FL, USA). The specific area (SA), average pore size (APS), and pore size diameter (PSD) were determined by the Brunauer-Emmet-Teller (BET) technique (Quantachrome Instruments, model 1000, Boynton Beach, FL, USA) through nitrogen adsorption isotherm at 77 K. The Fourier transform infrared (FTIR) spectroscopy was applied to analyze the functional groups present on the surface of the material; this analysis was performed using a spectrophotometer (Rayleigh, model WQF-510, Chelmsford, UK) between the range of 400 to 4000  $\text{cm}^{-1}$ . The spectrometry X-ray fluorescence (XRF) (Bruker, Model AXS GmbH, Ettlingen, Germany) allows us to identify the chemical elements present in a sample, as well as establish the proportion in which each one is present. The point of zero charge ( $\text{pH}_{\text{CZ}}$ ) experiment was performed according to the methodology of Ribeiro et al. (2019) [11].

### 2.3. Adsorption of Industrial Dyes

A preliminary study was conducted to compare the adsorption of methylene blue (MB), crystal violet (CV), indigo carmine (IC), bromocresol green (BG), and basic fuchsin (BF). The experiments were performed under the following conditions: 0.1 g adsorbent dosage, 25 mL dye solution with an initial dye concentration of 100 mg/L, at room temperature. The adsorption process was carried out in a rotatory shaker (Nova Ética, 109/1, São Paulo, Brazil) at 150 rpm for 1 h. Samples were centrifuged (QUÍMIS, Model Q222TM216, Caxias Do Sul, Brazil) at 4000 rpm for 10 min. The residual concentration of textile dyes was quantified using a UV-vis spectrophotometer (EQUILAM, UV 755B, Diadema, Brazil) at the maximum wavelength indicated in Table 2. The adsorption capacity and percentage removal of each dye were calculated using Equations (1) and (2), where  $C_0$  is the initial dye concentration (mg/L),  $C_e$  is the equilibrium dye concentration (mg/L),  $m$  is the mass adsorbent (g),  $V$  is the volume of the dye solution (L), and  $q_e$  is the adsorption capacity at equilibrium (mg/g).

$$q_e = \frac{C_0 - C_e}{C_0} V \quad (1)$$

$$\text{Dye removal}(\%) = \frac{(C_0 - C_e)}{m} V \times 100 \quad (2)$$

**Table 2.** Chemical structure, molar mass, and wavelength of industrial dyes.

Dye	Molar Mass (g/mol)	Nature	Wavelength (nm)
MB	319.85	Cationic	560
CV	407.98	Cationic	590
IC	466.36	Anionic	610
BG	698.01	Anionic	450
BF	337.86	Cationic	558

### 2.4. Kinetics and Equilibrium Adsorption

The kinetic experiments were conducted considering an adsorbent dosage of 0.1 g, and 25 mL dye solution with an initial dye concentration of 100 mg/L, at room temperature. The adsorption kinetic was performed in a rotary shaker (Nova Ética, 109/1) at 150 rpm for 0 to 20 min. Samples were centrifuged and analyzed in a UV-vis spectrophotometer ( $\lambda = 560$  nm). The kinetic models of pseudo-first-order (PFO) and pseudo-second-order (PSO) were fitted to the experimental data [43]. An equilibrium isotherms study was carried out using MB solution with an initial concentration from 25 to 225 mg/L, at 303 and 323 K. The results were fitted to the equilibrium models of Langmuir and Freundlich. The models are presented in Table 3.

**Table 3.** Kinetic and equilibrium adsorption models.

Model	Equation	Parameters
PFO	$q_t = q_e(1 - e^{-k_1 t})$	$q_e$ : equilibrium adsorption capacity (mg/g) $q_t$ : adsorption capacity (mg/g) $t$ : time t (min) $k_1$ : adsorption rate constant of PFO (1/min)
PSO	$q_t = \frac{q_e^2(k_2 t)}{(1 + q_e k_2 t)}$	$q_e$ : equilibrium adsorption capacity (mg/g) $q_t$ : adsorption capacity (mg/g) $t$ : time t (min) $k_2$ are the adsorption rate constant of PSO (g/mg·min <sup>-1</sup> )
Langmuir	$q_e = \frac{q_{max} C_e}{1 + k_L C_e}$	$q_{max}$ : maximum adsorption capacity (mg/g) $K_L$ : Langmuir constant (L/mg)
Freundlich	$q_e = k_F C_e^{\frac{1}{n_F}}$	$q_{max}$ : maximum adsorption capacity (mg/g) $K_F$ : Freundlich constant (mg/g)/(mgL) <sup>-1/n<sub>F</sub></sup> $1/n_F$ : equilibrium constant

### 3. Results and Discussion

#### 3.1. Characterization of UC

The UC's specific mass (SM) was equivalent to 2.05 g/cm<sup>3</sup> (Table 4) in accordance with the literature [26,44]. This result confirms the great performance of the fraction separation process, based on the difference in specific mass between the UC and FA, which presents a specific mass in the range of 2.3 to 2.45 g/cm<sup>3</sup> [11,31]. The value obtained for UC was expected since the employment of high temperature in the gasification process promotes a decrease in the specific mass, which may be related to an increase in porosity [8,45]. The surface area (SA) was 23.984 m<sup>2</sup>/g, which is in the range of 16.5 to 58 m<sup>2</sup>/g obtained by other authors for UC [26,44,46]. Carbons derived from class F fly ash, which are obtained from the burning of low-calcium bituminous coal, normally have low surface areas when compared to active carbons [26,47].

**Table 4.** Physical properties of the UC.

Properties	SM (g/cm <sup>3</sup> )	SA (m <sup>2</sup> /g)	APD (nm)	PV (cm <sup>3</sup> /g)	CV (cal/g)
UC	2.054 ± 0.002	23.984	0.844	2.262	4691 ± 11

The measurement of pore diameter (APD) was 0.844 nm, which is similar to the range indicated by the literature and, according to IUPAC, is classified as a micropore (<2 nm) [48]. The low SA can also be explained by the number of pores as well as by the low APD and PV, as these properties are related to each other [44]. Based on the calorimetric analysis, it was possible to observe an increase in the CV when compared to the coal from the Candiota mine, which presented values in the range of 3847.7 to 4701.8 cal/g. Table 5 shows the calorimetric analysis.

**Table 5.** Colorimetric analysis.

	UC	RC	FA <sup>1</sup>
$L$	28.45	31.25	10.34
$a^*$	0.41	0.48	1.87
$b^*$	0.36	0.19	8.78

<sup>1</sup> Raupp et al. (2022) [45].  $a^*$ : axis green/red chromaticity,  $b^*$ : axis blue/yellow chromaticity.

The colorimetric analysis indicated a tendency of the UC to be black in color as the value obtained for the  $L^*$  parameter was lower than 28.44. This result can be related to the success of FA separation since the colorimetric analysis can be used as a technique to

identify the presence, or not, of UC [49]. Based on these authors, a lighter sample indicates higher content of UC. The authors of [12] presented a colorimetric analysis of FA, obtaining an  $L^*$  value of 10.34, which, compared to the value obtained in the present work and according to other literature [12], indicates an increase in UC content after the decantation process. Analyzing the data obtained, it is possible to observe an increase in  $L^*$  value in the order  $RC > UC > FA$ , which is in accordance with another study [49], as this order follows the same tendency of the gasification process, where the raw material (RC) is the lightest, followed by the other products (UC and FA).

Figure 1 shows the FTIR spectra, which present peaks similar to the ones obtained by the literature [50] when analyzing high-density coal ( $>1.8 \text{ g/cm}^3$ ). First, it is possible to observe at approximately  $3600 \text{ cm}^{-1}$  (OH stretching region) four bands that are characteristic of the kaolinite compound [50–53]. The first one is located at  $3620 \text{ cm}^{-1}$  representing the inner hydroxyl groups; then the peaks at  $3653$  and  $3669 \text{ cm}^{-1}$  indicate the in-phase symmetric stretching vibration and  $3695 \text{ cm}^{-1}$  the out-of-phase stretching vibration [52]. The peaks at  $2929$  and  $2853 \text{ cm}^{-1}$  (Figure 2) indicate  $\text{CH}_2$  asymmetric and symmetric stretching vibration, respectively [50,54]. The low intensity of the peak at  $2929 \text{ cm}^{-1}$  may be related to the fact that the proportion of aliphatic  $-\text{CH}_3$  hydrogen is substituted by hydroxyl groups [53]. The  $1438 \text{ cm}^{-1}$  peak represents the  $\text{CH}_3$  asymmetric deformation vibration [50,53,54]. The peaks at  $934$  and  $915 \text{ cm}^{-1}$  may be related to the hydroxyl group in the carboxylic acid structure and phenolic hydroxyl group, respectively [50,55]. The peak located at  $777 \text{ cm}^{-1}$  is related to Si-O-Si bending vibration [56], and the band in the region near  $600 \text{ cm}^{-1}$  denotes the bending of Si-OH groups [57].

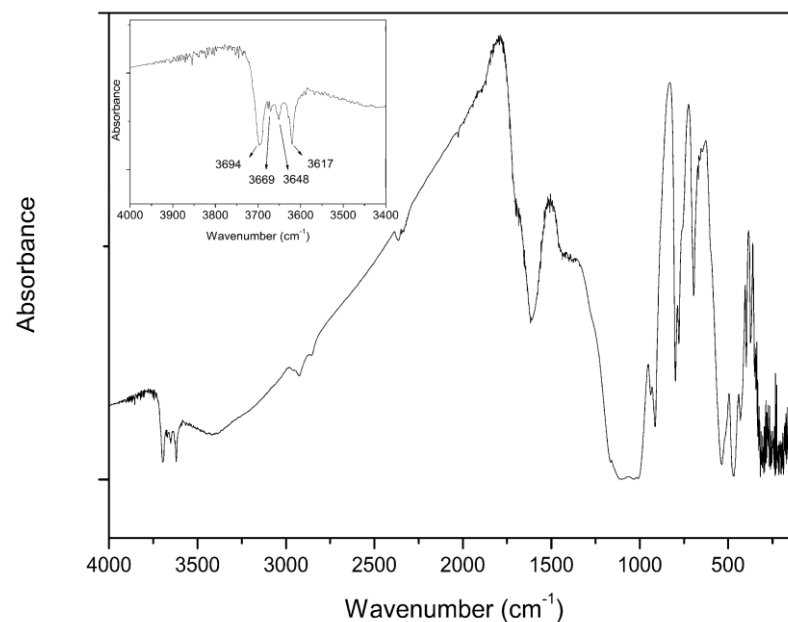


**Figure 1.** FTIR spectra of the UC.

The fluorescence X-ray analysis (Table 6) indicated that the UC is mainly composed of mineral compounds, such as  $\text{SiO}_2$ ,  $\text{Al}_2\text{O}_3$ , and  $\text{Fe}_2\text{O}_3$ , corroborating the information indicated by the FT-IR spectrum, and the results obtained for high-carbon FA [28]. When compared to coal from the same mine, it is possible to observe that after the separation there is a decrease in mineral content, which was expected due to the separation process from FA.

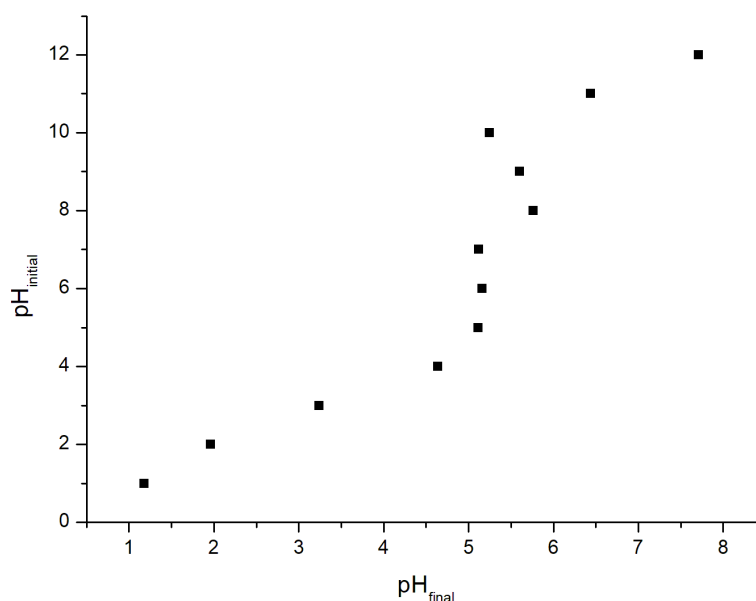


Figure 2. UC point of zero charge.

Table 6. FRX results of the chemical composition of UC.

Element	UC
SiO <sub>2</sub>	45.20
Al <sub>2</sub> O <sub>3</sub>	14.20
Fe <sub>2</sub> O <sub>3</sub>	3.03
CaO	2.03
K <sub>2</sub> O	1.64
MgO	1.02
TiO <sub>2</sub>	0.559
MnO	0.0657

The  $pH_{CZ}$  was 5.1, as indicated in Figure 2, which means that, in solutions with pH lower than this value, the adsorbent surface presents a positive charge, and at a higher pH value it has a negative charge. This value was similar to the results obtained by other authors, with  $pH_{CZ}$  equivalent to values lower than 7 [24,58]. The UC presented a wide range of pH values above the  $pH_{CZ}$ , indicating that it has favorable characteristics for interaction with cationic dyes, such as MB, CV, and BF [11,24,58]. The industrial conditions of UC production lead to acid functional group formation, such as carboxylic, lactonic, phenolic, and acyls in acid anhydrides, and neutral groups, such as carbonyl functional groups on the UC surface, as indicated by the FTIR analysis, which confirms its ability to interact with positively charged molecules [16].

Figures 3 and 4 present the adsorption capacity and removal of industrial dyes, which show results in the following order: IC (1.66 mg/g) < BG (5.84 mg/g) < BF (13.83 mg/g) < MB (16 mg/g) < CV (16.34 mg/g). It is possible to notice that the UC allowed the more efficient removal of cationic dyes, such as CV, MB, and BF in accordance with the information presented by the  $pH_{CZ}$  analysis. However, there is a difference between the values obtained for these dyes, and this behavior may be associated with molecule dye dimensions, as well as the charge effect indicated previously by the PCZ study [24]. As reported by the literature, CV adsorption occurs through a bond between dye and oxygen atoms present on SiO<sub>2</sub> and Al<sub>2</sub>O<sub>3</sub> [59], which, as reported by FRX analysis, were the major mineral compounds present in the UC. Reported adsorption capacity values were in the range of 33.46 to 80.36 mg/g for CV when applying an adsorbent material similar to UC. The difference between these values and those observed in the present study may be related to the employment of higher temperatures in the literature [58]. With regard to

the MB adsorption onto UC, the literature has reported values near 79.96 mg/g, and the difference between this value and the one obtained in the present study may be related to the gasification conditions, which play an important role in adsorbent properties, such as surface functional groups, pore volume and size, surface area, and others [60,61]. The literature has indicated adsorption capacity values of BF in the range of 7.16 to 34 mg/g by material with similar properties to UC [51]. The values obtained for BG and IC are in agreement with values reported by other authors and may be related to the anionic nature of these dyes [62].

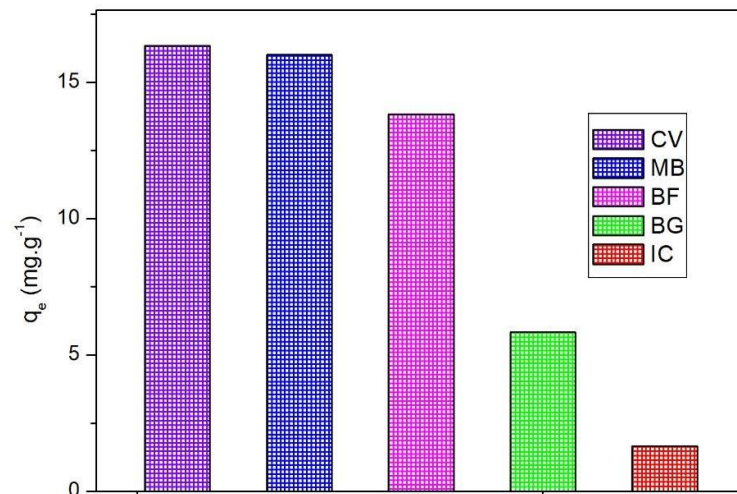


**Figure 3.** Comparison of experimental adsorption of different textile dyes (capacity).

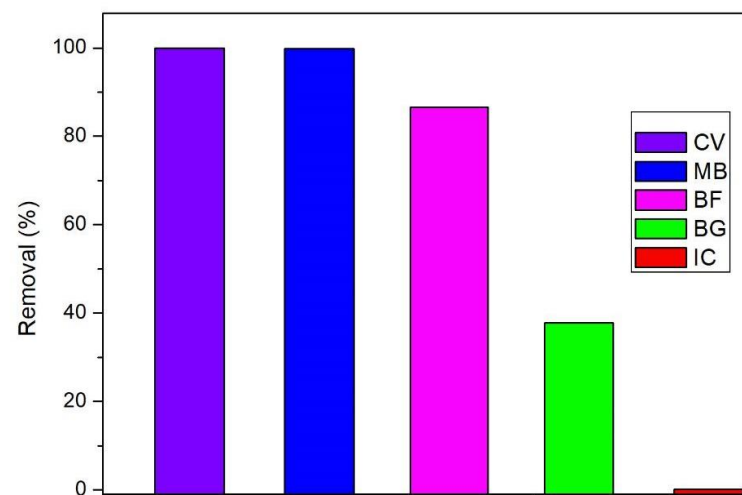


**Figure 4.** Comparison of experimental adsorption of different textile dyes (removal).

Figure 5 presents the kinetic data, which indicates that the first step of the adsorption process is characterized by a fast increase in dye adsorption capacity within the first five minutes. According to the literature, this may be related to the occupation of available adsorption sites at the beginning, which leads to a higher difficulty for other dye molecules to be adsorbed due to repulsion forces between the adsorbent and the dye surface [63]. Considering the high adsorption rate, it is possible to assume that the process adsorptive was determined mostly by the mass transfer mechanism convective, which was confirmed by the kinetic model fitting (Table 7). It is possible to observe that the adsorption capacity at equilibrium was equal to almost 50 mg/g, which is lower than the value obtained by Wang et al. [58] and must be related to the adsorbent dosage since the adsorption capacity may be related to the availability of adsorption sites.

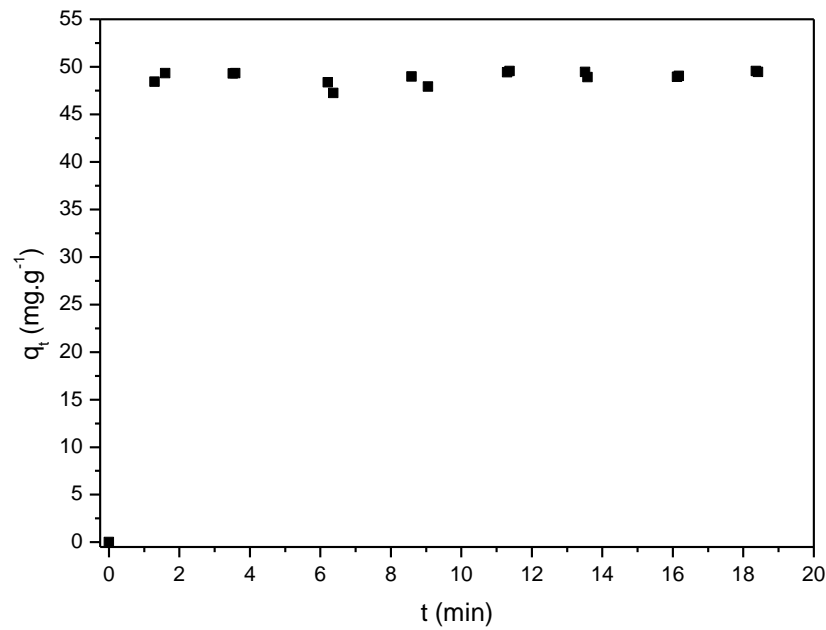


Figure 5. Effect of contact time on MB 100 mg·L<sup>-1</sup> adsorption rate (pH 7.0 at 298 K).

Table 7. Kinetic parameters for the MB adsorption onto UC.

PFO	$q_e$ (mg/g)	$k_1$ (min <sup>-1</sup> )	$R^2$
	49.0858	3.5609	0.9996
PSO	$q_e$ (mg/g)	$k_2$ (g/mg·min)	$R^2$
	49.4071	0.3080	0.9999

The two kinetic models showed a good fit to the experimental data with high correlation coefficients ( $R^2 > 0.999$ ); however, the PSO model presented the best fit. This result is consistent with those observed by other authors in their studies on the adsorption kinetics of dyes on UC [24,35,51,64,65]. The PSO model describes an adsorption process that occurs on a heterogeneous surface which has a random distribution and, also, indicates that the interaction between dye and adsorbate is chemical, which involves the sharing or exchange of electrons [59,66,67]. The fact that the adsorption process is mainly governed by chemisorption is related to the electrostatic interaction between the dye and the UC, which occurs due to the cationic nature of MB and the UC surface composed of negative charges. Another important aspect is the difference between the UC pore diameter and the MB molecule size. According to the characterization analysis, the UC has smaller pores than the MB molecule, which is unfavorable for diffusion adsorption and suggests surface adsorption related to a convective adsorption mechanism [68,69].

The equilibrium value  $k_2$  is related to the adsorption rate, and the low value observed by the fit is in agreement with the fact that the system reaches equilibrium quickly. This result may be related to the high active sites and the O-containing functional groups on the surface of UC, which improve the electrostatic relationship between the UC and MB molecules [70].

### 3.2. Adsorption Isotherms

The adsorption studies were conducted at two different temperatures, 303 and 328 K to evaluate the influence of temperature on the adsorption process; the experimental data are shown in Figure 6.

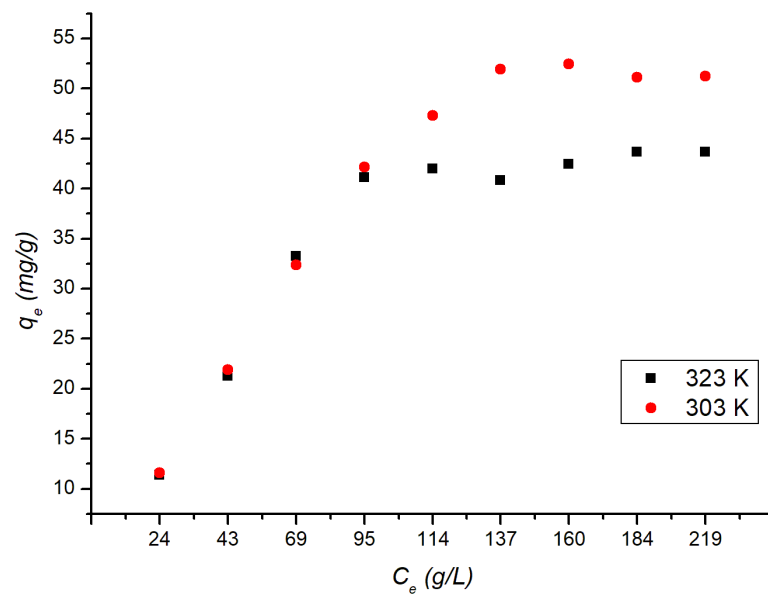


**Figure 6.** Effect of initial dye concentration on the removal of MB by UC at various temperatures (303 and 328 K).

According to IUPAC classification, the isotherms shown below may be classified as Type I, which is considered reversible and is given to microporous solids with small external surfaces, information that is in accordance with the results obtained through the BET analysis [48]. It was possible to observe that the Freundlich model presented the best fit for the lowest temperature of 218 K, which was also observed by other authors in a study regarding the adsorption of Naphthol Green B on UC at a temperature of 273 K [46]. This result (Table 8) suggests that the surface and pores of the UC are heterogeneous at lower temperatures, have non-uniform heat distribution and adsorption affinities, and have a multilayer adsorption mechanism [24,70–73].

**Table 8.** Equilibrium isotherm parameters for MB adsorption onto UC.

Isotherm	Parametric	291 K	328 K
Langmuir	$q_{max}$ (mg/g)	333.3333	476.1905
	$k_L$ (L/mg)	0.1209	0.2692
	$R_L$	0.0136	0.0061
	$R^2$	0.7705	0.9194
Freundlich	$n_F$	0.9151	1.5949
	$K_F$ (mg/g)(mg/L) <sup>-1/n<sub>F</sub></sup>	5.4843	4.6511
	$R^2$	0.93	0.9164

It is possible to observe a decrease in the value of  $k_F$  with increasing temperature. The value of  $k_F$  obtained at 291 and 328 K were, respectively, 5.48 and 4.65, which indicates the higher the temperature, the more favorable is the adsorption process [74]. The value of  $n$  indicates heterogeneity, with  $n$  higher than one ( $n > 1$ ) [75]. For the maximum temperature of 328 K, the  $n$  obtained was 1.91. Thus, the higher the temperature, the less favorable it is to multilayer adsorption, and at a higher temperature, the behavior of the adsorbent will be heterogeneous. For the maximum temperature of 328 K, the best model was the Langmuir model, with a maximum adsorption capacity of 476 mg/g, higher than those reported by other authors in their studies on the adsorption of MB onto FA and UC [24,32]. It is possible to observe an increase in maximum adsorption capacity with the temperature, which can be related to an increase in the rate of diffusion of the adsorbate, also observed by Wang and Li [24]. According to the  $R_L$  value, determined through the Langmuir parameters, it is possible to observe that the isothermal form is favorable at both temperatures presented in

the present work, given that  $0 < R_L < 1$  [71]. The  $k_L$  is a constant that may be related to the adsorption energy. In a study conducted by another author on methylene adsorption, it was observed that the  $k_L$  values ranged from 0.21 to 0.48 [60]. In the present study, at the temperature of 328 K, the best fit was the Langmuir model, obtaining a value of 0.26 for  $k_L$ . The results obtained indicate that the MB adsorption mechanism onto UC is related to the temperature.

#### 4. Conclusions

It was possible to recover UC from FA by a simple and easy methodology. UC was shown to be an effective low-cost adsorbent for removing textile dyes from aqueous solutions due to its properties, such as high SA, average pore diameter, and pore volume of 23.984 m<sup>2</sup>/g, 0.844 nm, and 2.262 cm<sup>3</sup>/g, respectively. The characterization also indicated the presence of hydroxyl and carbonyl functional groups on the UC surface, which leads to great performance in cationic dye adsorption, in accordance with the pH<sub>CZ</sub>. The UC was effective in the adsorption of CV, MB, and BF, reaching almost 80% removal. The kinetic model with the best fit was the pseudo-second-order, indicating a chemisorption mechanism between the dye and UC. Regarding the adsorption isotherm, it was observed that the Freundlich and Langmuir models fitted better at 291 and 328 K, respectively, indicating that increases in temperature promote the homogeneity of heat distribution on the adsorbent surface, as well as leading to a monolayer adsorption mechanism. It can be concluded that UC is a material with interesting properties as an adsorbent material, indicating an effective alternative for its reuse. Therefore, further studies are required with the aim of optimizing the experimental conditions of adsorption onto UC.

**Author Contributions:** Conceptualization: G.L. and T.L.R.; methodology: G.L. and T.L.R.; formal analysis: G.L. and T.L.R.; investigation: G.L. and T.L.R.; resources: G.L., G.S.d.R., T.L.R. and A.R.C.M.; writing—original draft preparation: G.L. and T.L.R.; writing—review: G.S.d.R., A.R.C.M. and J.V.d.R.; editing: G.L. and T.L.R.; supervision: G.S.d.R. and A.R.C.M.; Project administration: A.R.C.M.; Funding acquisition: A.R.C.M. All authors have read and agreed to the published version of the manuscript.

**Funding:** This research received no external funding.

**Data Availability Statement:** Data available upon request.

**Acknowledgments:** The authors would like to acknowledge the support of the Energy and Carbochemistry Laboratory, the Particulate Systems Research Group, and the Federal University of Pampa. The study also received support from Companhia Riograndense de Mineração—CRM (Mining Company of Rio Grande do Sul), which provided the coal needed for laboratory tests.

**Conflicts of Interest:** The authors declare no conflict of interest.

#### References

1. Wang, W.; Fan, L.; Zhou, P. Evolution of global fossil fuel trade dependencies. *Energy* **2022**, *238*, 121924. [CrossRef]
2. BP, Statistical Review of World Energy, 2021. Available online: <https://www.epe.gov.br/pt> (accessed on 18 January 2022).
3. Bonifácio, A.D.S.; Brum, R.D.L.; Tavella, R.A.; Ramires, P.F.; Lessa, I.M.; dos Santos, M.; Júnior, F.M.R.D.S. Human health risk assessment of metals and anions in surface water from a mineral coal region in Brazil. *Environ. Monit. Assess.* **2021**, *193*, 567. [CrossRef] [PubMed]
4. Associação Brasileira Do Carvão Mineral. Available online: <https://abcm.satc.edu.br/> (accessed on 27 May 2021).
5. Rodrigues, R.; Muniz, A.; Marcilio, N.R. Evaluation of biomass and coal co-gasification of brazilian feedstock using a chemical equilibrium model. *Braz. J. Chem. Eng.* **2016**, *33*, 401–414. [CrossRef]
6. Guo, Y.; Ma, C.; Zhang, Y.; Zhou, L.; Guo, Z.; Miao, Z.; Zhao, X.; Wu, J.; Guo, F. Comparative study on the structure characteristics, combustion reactivity, and potential environmental impacts of coal gasification fine slag with different particle size fractions. *Fuel* **2022**, *311*, 122493. [CrossRef]
7. Midilli, A.; Kucuk, H.; Topal, M.E.; Akbulut, U.; Dincer, I. A comprehensive review on hydrogen production from coal gasification: Challenges and Opportunities. *Int. J. Hydrogen Energy* **2021**, *46*, 25385–25412. [CrossRef]
8. Aineto, M.; Acosta, A.; Rincón, J.M.; Romero, M. Thermal expansion of slag and fly ash from coal gasification in IGCC power plant. *Fuel* **2006**, *85*, 2352–2358. [CrossRef]
9. Pandian, N.S. Fly ash characterization with reference to geotechnical applications. *J. Indian Inst. Sci.* **2004**, *84*, 189.

10. Nathan, Y.; Dvorachek, M.; Pelly, I.; Mimran, U. Characterization of coal fly ash from Israel. *Fuel* **1999**, *78*, 205–213. [[CrossRef](#)]
11. Ribeiro, P.B.; de Freitas, V.O.; Machry, K.; Muniz, A.R.C.; da Rosa, G.S. Evaluation of the potential of coal fly ash produced by gasification as hexavalent chromium adsorbent. *Environ. Sci. Pollut. Res.* **2019**, *26*, 28603–28613. [[CrossRef](#)]
12. Raupp, I.N.; Valério Filho, A.; Rodrigues, T.L.; Tholozan, L.V.; Luz, B.M.; Muniz, A.R.C.; Meili, L.; Rosa, G.S.; Almeida, A.R.F. *Novel Materials for Environmental Remediation Applications*, 1st ed.; Giannakoudakis, D.A., Meili, L., Anastopoulos, I., Eds.; Elsevier: Amsterdam, The Netherlands, 2022.
13. Bhatt, A.; Priyadarshini, S.; Mohanakrishnan, A.A.; Abri, A.; Sattler, M.; Techapaphawit, S. Physical, chemical, and geotechnical properties of coal fly ash: A global review. *Case Stud. Constr. Mater.* **2019**, *11*, e00263. [[CrossRef](#)]
14. Flores, C.G.; Schneider, H.; Marcilio, N.R.; Ferret, L.; Oliveira, J.C.P. Potassic zeolites from Brazilian coal ash for use as a fertilizer in agriculture. *Waste Manag.* **2017**, *70*, 263–271. [[CrossRef](#)] [[PubMed](#)]
15. Estevam, S.T.; de Aquino, T.F.; da Silva, T.D.; da Cruz, R.; Bonetti, B.; Riella, H.G.; Soares, C. Synthesis of K-Merlinoite zeolite from coal fly ash for fertilizer application. *Braz. J. Chem. Eng.* **2021**, *39*, 631–643. [[CrossRef](#)]
16. Kisiela-Czajka, A.M.; Hull, S.; Albinia, A. Investigation of the activity of unburned carbon as a catalyst in the decomposition of NO and NH<sub>3</sub>. *Fuel* **2022**, *309*, 122170. [[CrossRef](#)]
17. Rezaei, H.; Shafaei, S.Z.; Abdollahi, H.; Shahidi, A.; Ghassa, S. A sustainable method for germanium, vanadium and lithium extraction from coal fly ash: Sodium salts roasting and organic acids leaching. *Fuel* **2022**, *312*, 122844. [[CrossRef](#)]
18. Karanac, M.; Đolić, M.; Veljović, Đ.; Rajaković-Ognjanović, V.; Veličković, Z.; Pavičević, V.; Marinković, A. The removal of Zn<sup>2+</sup>, Pb<sup>2+</sup>, and As(V) ions by lime activated fly ash and valorization of the exhausted adsorbent. *Waste Manag.* **2018**, *78*, 366–378. [[CrossRef](#)]
19. Adamczyk, Z.; Komorek, J.; Białecka, B.; Catus-Moszko, J.; Klupa, A. Possibilities of Graphitization of Unburned Carbon from Coal Fly Ash. *Minerals* **2021**, *11*, 1027. [[CrossRef](#)]
20. Popławski, J.; Lelusz, M. Assessment of Sieving as a Mean to Increase Utilization Rate of Biomass Fly Ash in Cement-Based Composites. *Appl. Sci.* **2023**, *13*, 1659. [[CrossRef](#)]
21. David, E.; Kopač, J. Efficient removal of tar from gas fraction resulting from thermo-chemical conversion of biomass using coal fly ash-based catalysts. *Renew. Energy* **2021**, *171*, 1290–1302. [[CrossRef](#)]
22. Guo, F.; Miao, Z.; Guo, Z.; Li, J.; Zhang, Y.; Wu, J. Properties of flotation residual carbon from gasification fine slag. *Fuel* **2020**, *267*, 117043. [[CrossRef](#)]
23. Zhang, R.; Guo, F.; Xia, Y.; Tan, J.; Xing, Y.; Gui, X. Recovering unburned carbon from gasification fly ash using saline water. *Waste Manag.* **2019**, *98*, 29–36. [[CrossRef](#)]
24. Wang, S.; Li, H. Dye adsorption on unburned carbon: Kinetics and equilibrium. *J. Hazard. Mater.* **2005**, *126*, 71–77. [[CrossRef](#)] [[PubMed](#)]
25. Badenhorst, C.; Wagner, N.; Valentim, B.; Viljoen, F.; Santos, A. Separation of unburned carbon from coal conversion ash: Development and assessment of a dry method. *Coal Combust. Gasif. Prod.* **2019**, *11*, 89–96. [[CrossRef](#)]
26. Baltrus, J.P.; Wells, A.W.; Fauth, D.J.; Diehl, J.R.; White, C.M. Characterization of Carbon Concentrates from Coal-Combustion Fly Ash. *Energy Fuels* **2001**, *15*, 455–462. [[CrossRef](#)]
27. Wierchowski, K.; Białecka, B.; Moszko, J.C.; Klupa, A. Characterization of unburned carbon separated from power plant slag. *Int. J. Environ. Sci. Technol.* **2020**, *17*, 2499–2510. [[CrossRef](#)]
28. Altynsary, B.; Saule, A.; Ablay, Z.; Natalya, O. Preliminary Chemical Activation of Ash Waste with Release of Carbon Concentrate. *Chem. Eng. Trans.* **2021**, *88*, 973–978. [[CrossRef](#)]
29. Yang, Z.; Chang, G.; Xia, Y.; He, Q.; Zeng, H.; Xing, Y.; Gui, X. Utilization of waste cooking oil for highly efficient recovery of unburned carbon from coal fly ash. *J. Clean. Prod.* **2020**, *282*, 124547. [[CrossRef](#)]
30. Lin, H.; Takasu, K.; Koyamada, H.; Suyama, H. Development of Flotation Device for Removing Unburnt Carbon in Fly Ash for Use in Hardened Cementitious Materials. *Materials* **2021**, *14*, 6517. [[CrossRef](#)]
31. Masoomi, I.; Kamata, H.; Yukimura, A.; Ohtsubo, K.; Schmid, M.O.; Scheffknecht, G. Investigation on the behavior of mercury across the flue gas treatment of coal combustion power plants using a lab-scale firing system. *Fuel Process. Technol.* **2020**, *201*, 106340. [[CrossRef](#)]
32. Rosa, T.; Martins, A.; Santos, M.; Trindade, T.; Nunes, N. Coal Fly Ash Waste, a Low-Cost Adsorbent for the Removal of Mordant Orange Dye from Aqueous Media. *J. Braz. Chem. Soc.* **2021**, *32*, 2245–2256. [[CrossRef](#)]
33. Rubio, B.; Izquierdo, M.T.; Mayoral, M.C.; Bona, M.T.; Andres, J.M. Unburnt carbon from coal fly ashes as a precursor of activated carbon for nitric oxide removal. *J. Hazard. Mater.* **2006**, *143*, 561–566. [[CrossRef](#)]
34. Singh, K.; Kumar, A.; Singh, A.K.; Agarwal, A. Fly ash and TiO<sub>2</sub> modified fly ash as adsorbing materials for effective removal of methylene blue and malachite green from aqueous solutions. *J. Indian Chem. Soc.* **2023**, *100*, 100942. [[CrossRef](#)]
35. Wang, S.; Ma, Q.; Zhu, Z. Characteristics of unburned carbons and their application for humic acid removal from water. *Fuel Process. Technol.* **2009**, *90*, 375–380. [[CrossRef](#)]
36. Alkurdi, S.S.; Herath, I.; Bundschuh, J.; Al-Juboori, R.A.; Vithanage, M.; Mohan, D. Biochar versus bone char for a sustainable inorganic arsenic mitigation in water: What needs to be done in future research? *Environ. Int.* **2019**, *127*, 52–69. [[CrossRef](#)] [[PubMed](#)]
37. Li, W.; Mu, B.; Yang, Y. Feasibility of industrial-scale treatment of dye wastewater via bio-adsorption technology. *Bioresour. Technol.* **2019**, *277*, 157–170. [[CrossRef](#)] [[PubMed](#)]

38. Benjelloun, M.; Miyah, Y.; Evrendilek, G.A.; Zerrouq, F.; Lairini, S. Recent Advances in Adsorption Kinetic Models: Their Application to Dye Types. *Arab. J. Chem.* **2021**, *14*, 103031. [[CrossRef](#)]
39. *NBR 10850*; Carvão Mineral—Análise Química Das Cinzas Por Complexometria, Fotometria De Chama, Espectrocolorimetria E Gravimetria. Associação Brasileira de Normas Técnicas: Rio de Janeiro, Brazil, 1989.
40. *AS 1038.5*; Coal and Coke—Analysis and Testing Gross Calorific Value. Standards Australia: Homebush, Australia, 1949.
41. *NBR 12076*; Carvão Ativado Pulverizado—Determinação da Massa Específica Aparente—Método de Ensaio. Associação Brasileira de Normas Técnicas: Rio de Janeiro, Brazil, 1981.
42. *E1252*; Standard Practice for General Techniques for Obtaining Infrared Spectra for Qualitative Analysis. American Society for Testing and Materials: West Conshohocken, PA, USA, 1998.
43. Raupp, I.N.; Filho, A.V.; Arim, A.L.; Muniz, A.R.C.; da Rosa, G.S. Development and Characterization of Activated Carbon from Olive Pomace: Experimental Design, Kinetic and Equilibrium Studies in Nimesulide Adsorption. *Materials* **2021**, *14*, 6820. [[CrossRef](#)]
44. Hsieh, Y.-M.; Tsai, M.-S. Physical and chemical analyses of unburned carbon from oil-fired fly ash. *Carbon* **2003**, *41*, 2317–2324. [[CrossRef](#)]
45. Xing, Y.; Guo, F.; Xu, M.; Gui, Z.; Li, H.; Xia, Y.; Han, H. Separation of unburned carbon from coal fly ash. A review. *Powder Technol.* **2019**, *216*, 866–882. [[CrossRef](#)]
46. Bartoňová, L.; Klika, Z.; Spears, D. Characterization of unburned carbon from ash after bituminous coal and lignite combustion in CFBs. *Fuel* **2007**, *86*, 455–463. [[CrossRef](#)]
47. Kūlaots, I.; Hurt, R.H.; Suuberg, E.M. Size distribution of unburned carbon in coal fly ash and its implications. *Fuel* **2004**, *83*, 223–230. [[CrossRef](#)]
48. Thommes, M.; Kaneko, K.; Neimark, A.V.; Olivier, J.P.; Rodriguez-Reinoso, F.; Rouquerol, J.; Sing, K.S.W. Physisorption of gases, with special reference to the evaluation of surface area and pore size distribution (IUPAC Technical Report). *Pure Appl. Chem.* **2015**, *87*, 1051–1069. [[CrossRef](#)]
49. Kizil, M.; Peterson, J.; English, W. The effect of coal particle size on colorimetric analysis of roadway dust. *J. Loss Prev. Process. Ind.* **2001**, *14*, 387–394. [[CrossRef](#)]
50. Xing, Y.; Gui, X.; Liu, J.; Cao, Y.; Zhang, Y.; Li, S. Flotation behavior of hard-to-separate and high-ash fine coal. *Physicochem. Probl. Miner. Process.* **2016**, *52*, 703–717. [[CrossRef](#)]
51. Yan, S.; Pan, Y.; Wang, L.; Liu, J.; Zhang, Z.; Huo, W.; Yang, J.; Huang, Y. Synthesis of low-cost porous ceramic microspheres from waste gangue for dye adsorption. *J. Adv. Ceram.* **2018**, *7*, 30–40. [[CrossRef](#)]
52. Sarkar, M.; Dana, K. Partial replacement of metakaolin with red ceramic waste in geopolymer. *Ceram. Int.* **2020**, *47*, 3473–3483. [[CrossRef](#)]
53. Balachandran, M. Role of Infrared Spectroscopy in Coal Analysis—An Investigation. *Am. J. Anal. Chem.* **2014**, *05*, 367–372. [[CrossRef](#)]
54. Jiang, J.; Zhang, S.; Longhurst, P.; Yang, W.; Zheng, S. Molecular structure characterization of bituminous coal in Northern China via XRD, Raman and FTIR spectroscopy. *Spectrochim. Acta Part A Mol. Biomol. Spectrosc.* **2021**, *255*, 119724. [[CrossRef](#)] [[PubMed](#)]
55. Zhang, W.; Jiang, S.; Wang, K.; Wang, L.; Xu, Y.; Wu, Z.; Shao, H.; Wang, Y.; Miao, M. Thermogravimetric Dynamics and FTIR Analysis on Oxidation Properties of Low-Rank Coal at Low and Moderate Temperatures. *Int. J. Coal Prep. Util.* **2015**, *35*, 39–50. [[CrossRef](#)]
56. Samah, K.; Sahar, M.; Yusop, M. Structural Properties of Cullet-Paper Ash-Kaolin Clay Ceramic. *J. Phys. Conf. Ser.* **2017**, *1083*, 012007. [[CrossRef](#)]
57. Bellamy, L.J. *The Infrared Spectra of Complex Molecules*; Chapman and Hall: London, UK, 1980. [[CrossRef](#)]
58. Wang, S.; Li, H. Kinetic modelling and mechanism of dye adsorption on unburned carbon. *Dye. Pigment.* **2007**, *72*, 308–314. [[CrossRef](#)]
59. Astuti, W.; Chafidz, A.; Wahyuni, E.T.; Prasetya, A.; Bendiyasa, I.M.; Abasaeed, A.E. Methyl violet dye removal using coal fly ash (CFA) as a dual sites adsorbent. *J. Environ. Chem. Eng.* **2019**, *7*, 103262. [[CrossRef](#)]
60. Vezentsev, A.I.; Thuy, D.M.; Goldovskaya-Peristaya, L.F.; Glukhareva, N.A. Adsorption of Methylene Blue on the Composite Sorbent Based on Bentonite-Like Clay and Hydroxyapatite. *Indones. J. Chem.* **2018**, *18*, 733–741. [[CrossRef](#)]
61. Tan, X.-F.; Zhu, S.-S.; Wang, R.-P.; Chen, Y.-D.; Show, P.-L.; Zhang, F.-F.; Ho, S.-H. Role of biochar surface characteristics in the adsorption of aromatic compounds: Pore structure and functional groups. *Chin. Chem. Lett.* **2021**, *32*, 2939–2946. [[CrossRef](#)]
62. Carvalho, T.E.M.; Fungaro, D.A.; Magdalena, C.P.; Cunico, P. Adsorption of indigo carmine from aqueous solution using coal fly ash and zeolite from fly ash. *J. Radioanal. Nucl. Chem.* **2011**, *289*, 617–626. [[CrossRef](#)]
63. Liu, X.; He, C.; Yu, X.; Bai, Y.; Ye, L.; Wang, B.; Zhang, L. Net-like porous activated carbon materials from shrimp shell by solution-processed carbonization and H<sub>3</sub>PO<sub>4</sub> activation for methylene blue adsorption. *Powder Technol.* **2018**, *326*, 181–189. [[CrossRef](#)]
64. Dogar, S.; Nayab, S.; Farooq, M.Q.; Said, A.; Kamran, R.; Duran, H.; Yameen, B. Utilization of Biomass Fly Ash for Improving Quality of Organic Dye-Contaminated Water. *ACS Omega* **2020**, *5*, 15850–15864. [[CrossRef](#)]
65. Hsu, T.-C. Adsorption of an acid dye onto coal fly ash. *Fuel* **2008**, *87*, 3040–3045. [[CrossRef](#)]

66. Macías-García, A.; Carrasco-Amador, J.P.; Encinas-Sánchez, V.; Díaz-Díez, M.; Torrejón-Martín, D. Preparation of activated carbon from kenaf by activation with H<sub>3</sub>PO<sub>4</sub>. Kinetic study of the adsorption/electroadsorption using a system of supports designed in 3D, for environmental applications. *J. Environ. Chem. Eng.* **2019**, *7*, 103196. [[CrossRef](#)]
67. Chakraborty, S.; Chowdhury, S.; Das Saha, P. Adsorption of Crystal Violet from aqueous solution onto NaOH-modified rice husk. *Carbohydr. Polym.* **2011**, *86*, 1533–1541. [[CrossRef](#)]
68. Jia, P.; Tan, H.; Liu, K.; Gao, W. Removal of Methylene Blue from Aqueous Solution by Bone Char. *Appl. Sci.* **2018**, *8*, 1903. [[CrossRef](#)]
69. Filippov, L.K. Multicomponent non-isothermal adsorption dynamics. *Chem. Eng. Commun.* **1994**, *127*, 75–107. [[CrossRef](#)]
70. Dalhatou, S.; Sali, M.; Tetteh, S.; Boubakari, A.; Talami, B.; Zeghioud, H.; Kane, A.; El Jery, A.; Assadi, A.A.; Obada, D.O. Sorbent and Photocatalytic Potentials of Local Clays for the Removal of Organic Xenobiotic: Case of Crystal Violet. *Catalysts* **2022**, *12*, 899. [[CrossRef](#)]
71. Alpat, S.K.; Özbayrak, Ö.; Alpat, Ş.; Akçay, H. The adsorption kinetics and removal of cationic dye, Toluidine Blue O, from aqueous solution with Turkish zeolite. *J. Hazard. Mater.* **2008**, *151*, 213–220. [[CrossRef](#)] [[PubMed](#)]
72. Sun, D.; Zhang, X.; Wu, Y.; Liu, X. Adsorption of anionic dyes from aqueous solution on fly ash. *J. Hazard. Mater.* **2010**, *181*, 335–342. [[CrossRef](#)] [[PubMed](#)]
73. Hasan, T.; Hossain, L.; Hossain, M.A. Mechanism of Basic Violet 3 Adsorption on Used Black Tea Leaves from Neutral Solution. *Int. J. Sci. Eng. Res.* **2017**, *8*, 1047–1055. [[CrossRef](#)]
74. Menezes, J.M.C.; Bento, A.M.D.S.; da Silva, J.H.; Filho, F.J.D.P.; da Costa, J.G.M.; Coutinho, H.D.M.; Teixeira, R.N.P. Equilibrium, kinetics and thermodynamics of lead (II) adsorption in bioadsorbent composed by *Caryocar coriaceum* Wittm barks. *Chemosphere* **2020**, *261*, 128144. [[CrossRef](#)]
75. Khuluk, R.H.; Rahmat, A.; Buhani, B.; Suharso, S. Removal of Methylene Blue by Adsorption onto Activated Carbon from Coconut Shell (*Cocos Nucifera* L.). *Indones. J. Sci. Technol.* **2019**, *4*, 229–240. [[CrossRef](#)]

**Disclaimer/Publisher's Note:** The statements, opinions and data contained in all publications are solely those of the individual author(s) and contributor(s) and not of MDPI and/or the editor(s). MDPI and/or the editor(s) disclaim responsibility for any injury to people or property resulting from any ideas, methods, instructions or products referred to in the content.